Journal of Materials Chemistry A

Accepted Manuscript

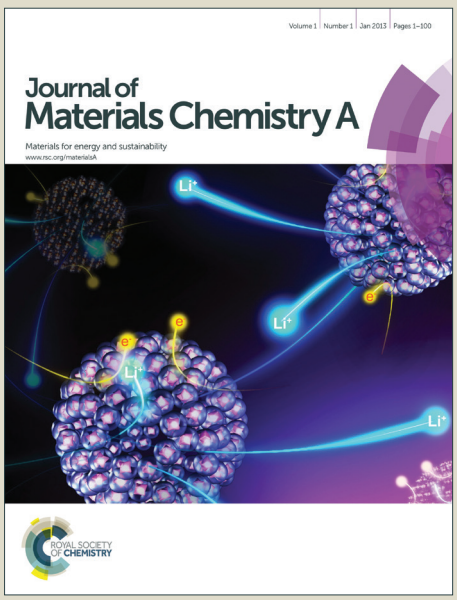

ROYAL SOCIETY OF CHEMISTRY

www.rsc.org/materialsA

Understanding compositions and electronic structures dependent photocatalytic performance of bismuth oxyiodides

Mingce Long*[a], Peidong Hu[a], Haodong Wu[b], Yuanyuan Chen[a], Beihui Tan[a], Weimin Cai[a, b]

[a]School of Environmental Science and Engineering, Shanghai Jiao Tong University, 800 Dong Chuan Road, Shanghai 200240, People's Republic of China

[b]Identity Environmental Technology (Shanghai) Co., Ltd., 555 Dong Chuan Road, Shanghai 200241, People's Republic of China

Corresponding author:

Mingce Long, Associate Professor, Dr.

Mail address: School of Environmental Science and Engineering, Shanghai Jiao Tong University, Dong Chuan Road 800, Shanghai 200240, People's Republic of China

Tel: 86-21-54747354

Fax: 86-21-54740825

Email: long_mc@sjtu.edu.cn

Abstract

A series of bismuth oxyiodides were obtained by calcining the precursor compound ($Bi_7O_9I_3$). Their compositions and electronic structures were analyzed by various physicochemical characterizations, slurry method measurements and theoretic calculations. Iodine vacancies appearing at elevated temperatures before the phase transition contribute to the increased photocatalytic activity, which can be attributed to the increase of band gaps, downward shifts of band potentials and the change of semiconductor behavior from p type toward n type. The catalyst obtained at 400 °C displayed an excellent photocatalytic performance for phenol degradation, and it was characterized as a composite of two components with well-matched band potentials and well contact interfaces. Photogenerated holes were revealed as the main active species in the phenol degradation. This study could bring insights in the fabrication of novel high efficient bismuth oxyiodide composites by simultaneously controlling the extent of phase transition and the amount of iodine vacancies.

Keywords: Bismuth oxyiodide; Photocatalysis; Heterojunction; Iodine vacancy; Visible light

Introduction

In recent decades, many new families of semiconductor photocatalysts, such as bismuth containing compounds ($BiVO_4$, Bi_2WO_6 and bismuth oxyhalides),[1-3] have been intensively investigated to target the conversion of solar energy and the removal of environmental pollutants. Bismuth oxyiodide is a type of main group V-VI-VII ternary oxide compounds with special layered crystal structure. In the lattice, positively charged $[Bi_2O_2]^{2+}$ slabs are interleaved by negative iodide slabs, resulting in an internal static electric field perpendicular to each layer. Such inherent electric fields are effective to facilitate the separation of photogenerated electron-hole pairs.[4-6] Therefore bismuth oxyiodides display promising photocatalytic performance both in wide spectrum response and in high efficiency. Up to now, several bismuth oxyiodide photocatalysts, including BiOI,[3, 7-9] $Bi_7O_9I_3$,[10] Bi_5O_7I,[11, 12] and $Bi_4O_5I_2$,[4, 5] has been synthesized and studied. Of these bismuth oxyiodides, only BiOI, $Bi_4O_5I_2$ and two phases of Bi_5O_7I have been structurally characterized.[13] Some bismuth oxyiodides, such as BiOI and $Bi_7O_9I_3$, are always confusable due to their similar XRD patterns and compositions. Among them, BiOI was firstly and most widely reported,[3] while $Bi_7O_9I_3$ was recently found to be the most efficient in these compounds.[4]

Generally, impurities and defects are frequently present in the solid materials. They have strong influence on geometric and electronic structures of the crystals, so as to result in various magnetic, optical, thermal, conductive and mechanical characteristics.[14-17] Due to the special layered structure of bismuth oxyiodides, iodine atoms in the lattice could easily get out or insert into the interlayer and form nonstoichiometric compounds with a broad range of Bi/I ratios. Iodine self-doped BiOI can be achieved by introducing overdosed iodine source in the syntheses, and the electronic structure and photocatalytic performance of such self-doping BiOI have been also reported by Zhang et al.[18]

However, there is little knowledge on the influence of iodine vacancies in bismuth oxyiodides, which could be facilely generated by calcinations. It was found that upon heating treatment, phase transition would take place to form oxygen rich bismuth oxyiodides, such as Bi_5O_7I, and finally become α-Bi_2O_3 at the higher temperature than 650 °C.[4, 19] The photocatalytic activities are also depends much on the calcination temperatures, even under the phase transition temperatures.[19] To the best of our knowledge, there is insufficient basic information on the changes of compositions and electronic structures of these catalysts with iodine vacancies.

On the other hand, fabricating heterojunctions by coupling two different semiconductors is a typical strategy to develop highly efficient photocatalytic nanostructures.[1, 20-25] At the interface of two components with matched band potentials, excited electrons and holes are prone to delocalize at different part, which would lead to a compartmentalization of interfacial reduction and oxidation, and result in more efficient photocatalytic reactions.[21] However, it is a challenge to make a well alloyed interface, which is essentially important to make charges migrate more fluently across the interface, and make charge separation more efficient.[24, 25] Wang et al. developed a Cr-doped $Ba_2In_2O_5/In_2O_3$ composite with a well alloyed interface by a solid-state reaction method from the corresponding precursor oxides.[24] Kim et al. introduce a metallic W interlayer as the ohmic junction layer to facilitate the charge transfer between WO_3 and $PbBi_2Nb_{1.9}Ti_{0.1}O_9$ composite.[25] However, interface with excellent contact could more possibly be generated in bismuth oxyiodides due to the consecutive loss of iodine followed with phase transition under calcinations. In this study, a series of bismuth oxyiodides have been obtained by thermally treating the precursor bismuth oxyiodide ($Bi_7O_9I_3$), the compositions and electronic structures of corresponding compounds have been analyzed, and the contributions of iodine vacancies and heterojunctions to the enhanced photocatalytic performance have

been revealed.

Experimental

The precursor bismuth oxyiodide (BOI-160) was synthesized by a solvothermal method.[5, 6] Briefly, 2.5 mmol bismuth nitrate was dissolved in 24 mL ethylene glycol under vigorous stirring, then equal amount of KI was added. The final solution was solvothermally heated in a 30 mL Teflon-lined stainless-steel autoclave at 160 °C for 12 hours. Finally, the resulting orange powder was filtrated, washed with de-ionized water and then dried at 80 °C. The prepared bismuth oxyiodide (BOI-160) was treated at various temperatures and denoted as BOI-T (T is the temperature). Bi_5O_7I was synthesized by a previously reported hydrothermal method.[11]

The crystal phases of the catalysts were analyzed using a powder X-ray diffraction (XRD, D/max-2200, Rigaku Corp.) with Cu Kα radiation, operating at 40 kV 30 mA (λ = 0.154 nm). A Lambda 950 UV/vis spectrophotometer (PerkinElmer Instrument Co., Ltd.) was used for diffuse reflectance spectra (DRS), and the reflectance was converted to absorption according to the Kubelka-Munk method. Data for elemental analyses were collected on an X-ray Fluorescence analyzer (XRF-1800, Shimadzu) with samples pressed into pellets. Thermal stability of BOI-160 was investigated by the thermogravimetric-differential thermal analysis (TG-DTA, TGA/DSC 1, Mettler Toledo) in the air atmosphere at a flow rate of 50 ml/min. The accuracy of weighing and temperature was within 0.1 μg and 0.2 °C, respectively. The heating program was set as: ramping at 5 °C/ min to 200 °C, 350 °C, 400 °C and 450 °C continuously, and holding at each point for 30 min; finally ramping to 600 °C at the rate of 5 °C/ min. X-ray photoelectron spectroscopy (XPS) experiments were taken on an AXIS Ultra DLD system produced by Shimadu-Kratos Company. A high resolution-transmission electron microscopy (HRTEM, JEM-2100F, JEOL, Japan) was used to observe the morphology of catalysts.

Photocatalytic performance of the catalysts were evaluated by phenol degradation under visible light from a 1000 W xenon lamp with a cutoff filter ($\lambda > 400$ nm). In a typical test, 0.05 g catalyst was added into a 50 mL phenol solution (initial concentration 10 mg/L). The suspension was previously stirred in the dark for 15 min to reach an adsorption equilibrium. During irradiation, samples were taken at regular time intervals, filtered, and then monitored by a colorimetry on a UNICO UV-2102 spectrometer at 510 nm.

Band potentials of catalysts were determined by the slurry method.[26] The suspension with 80 mg powder and 10 mg of $(MV)Cl_2$ (methylviologen dichloride, >98%, TCI) in a 80 mL KNO_3 aqueous solution (0.1 M) were irradiated by the full arc light of a 350 W Xe lamp with a glass filter to remove infrared light. The working and reference electrodes are a platinum plate and a saturated calomel electrode (SCE), respectively. Suspensions were magnetically stirred and flushed with N_2 during the measurement. Photovoltages were recorded at various pH values, which was adjusted by HNO_3 or NaOH solutions. If not specified, all potential values are given relative to normal hydrogen electrode (NHE).

First-principles calculations were performed within the density functional theory framework using a plane-wave basis set, and implemented in Quantum ESPRESSO.[27] The generalized gradient approximation (GGA) with Perdew-Burke-Ernzerhof (PBE) exchange-correlation functional, and norm-conserving pseudopotentials are used for all calculations. Wave functions were expanded in plane-waves with a kinetic energy cutoff of 80 Ry and 320 Ry for the smooth and augmented part of the density, respectively. Tetragonal BiOI, orthorhombic Bi_5O_7I and their corresponding compounds with iodine vacancies (the ratio of Bi/I are 1 or 4/3 for BiOI and 5 or 40/7 for Bi_5O_7I) were modeled and calculated. The Broyden–Fletcher–Goldfarb–Shanno (BFGS) geometry optimization scheme was

performed until forces and total electron energy converged below 0.001 eV/Å and 10^{-9} Ry, respectively.

Result and discussion

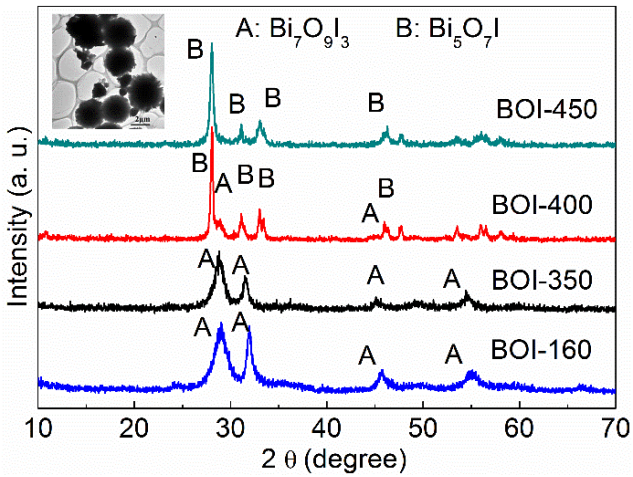

Fig. 1. XRD patterns of various bismuth oxyiodide catalysts. Inset is the TEM image of as-prepared BOI-160.

According to XRD patterns in Fig. 1, the characteristic peak at 28.8° in the as-prepared bismuth oxyiodide (BOI-160) is much different from the 29.7° for (102) plane of tetragonal phase BiOI (JCPDS 10-0445). The molecular ratio of Bi and I in this bismuth oxyiodide was determined to be 2.36 by XRF analyzer (Table 1), which is close to that ratio in $Bi_7O_9I_3$, the most efficient visible light driven photocatalyst in the already known bismuth oxyiodides.[4, 10] These results indicate that the as-prepared bismuth oxyiodide by solvothermal treatment in ethylene glycol is $Bi_7O_9I_3$ but not BiOI, which is in consistent with the previous report.[5] Morphology of BOI-160 was characterized by TEM, as shown in the inset in Fig. 1. It displays a hierarchical microsphere with a diameter of about 5 μm, being assembled from many nanoplates.

Table 1. Bismuth and iodine ratio for various bismuth oxyiodides from XRF measurements

Catalysts	BOI-160		BOI-350		BOI-400		BOI-450	
Elements	Bi	I	Bi	I	Bi	I	Bi	I
Weight percentage (%)	79.62	20.33	82.27	17.66	87.45	12.12	92.78	7.22
Molecular ratio (Bi/I)	2.36		2.80		4.38		7.81	

The effect of heating temperatures on the structure and performance of bismuth oxyiodide was investigated. Under calcinations below 350 °C, there is negligible change in the XRD patterns. However, when calcined at 400 °C, BOI-160 shows obvious alternations toward orthorhombic structure Bi_5O_7I (JCPDS 40-0548). The phase transition has almost completed at 450 °C, because the XRD pattern of BOI-450 is exclusively identical to that of Bi_5O_7I. The phase transition of $Bi_7O_9I_3$ toward Bi_5O_7I can be described by Eq. 1. Although the crystal structure shows negligible change when calcined at 350 °C (Fig. 1), the decrease of iodine content in the catalyst was confirmed from the XRF analyses. The ratio of Bi to I increases from the initial 2.36 of BOI-160 to 2.80 of BOI-350, indicating abundant iodine vacancies generate during calcination at the temperatures before phase transitions. It should be noted that although there are about 16% iodine escaped from the crystal lattice after heating treated at 350 °C, BOI-350 still maintains a similar crystal structure as its precursor BOI-160.

$$5Bi_7O_9I_3 + 2O_2 \rightarrow 7Bi_5O_7I + 4I_2 \uparrow \qquad (1)$$

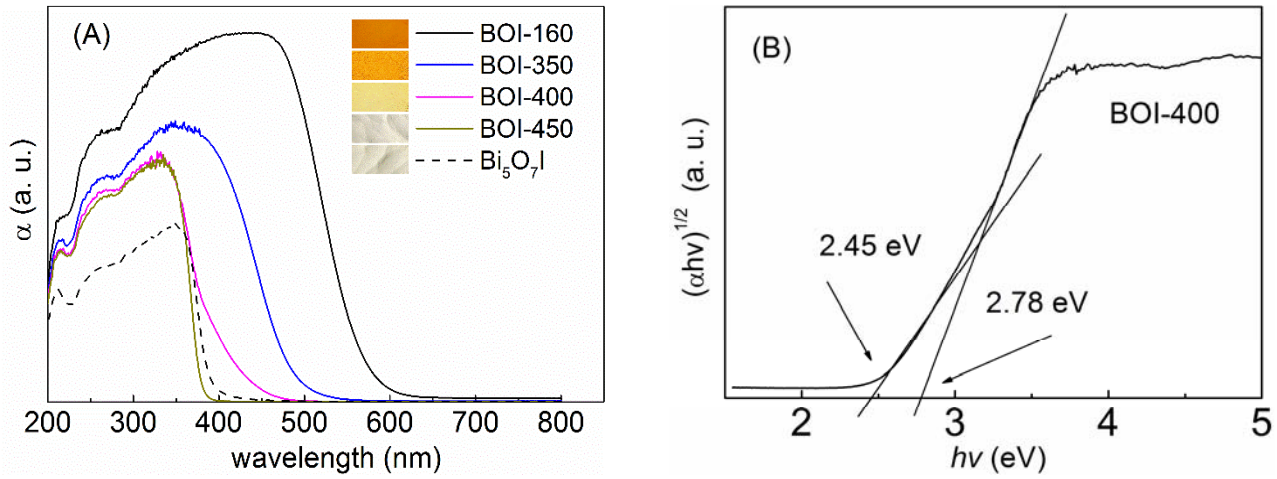

Fig. 2. (A) DRS spectra of various bismuth oxyiodide catalysts; (B) the plot of $(\alpha h\nu)^{1/2}$ versus the photon energy (hν) for BOI-400.

Accompanying with the loss of iodine at elevated temperatures, the colors of the catalysts change from dark red to brown, light yellow and then complete white. Fig. 2 shows the optical absorption properties of various catalysts. The apparent absorption edges of the catalysts downward shift obviously with the increase of calcination temperatures. Based on their indirect transition behavior and the linear relationships between $(\alpha h\nu)^{1/2}$ and the photon energy (hν), the band gap energies can be estimated as 2.04, 2.31, 2.61 and 3.18 eV for the BOI-160, BOI-350, BOI-400 and BOI-450, respectively. BOI-450 displays a slight larger band gap than the reported value for Bi_5O_7I (2.61-2.94 eV),[4, 11, 12] which can be attributed to the existence of iodine vacancies. As we observed from XRF (Table 1), the high ratio of Bi/I of 7.81 in BOI-450 suggests that a high concentration of iodine vacancies presents in the lattice. It is notable that the spectrum of BOI-400 displays two observable band absorptions, which can be fitted into two band gap energies of 2.45 and 2.78 eV. The former band gap absorption corresponds to the bismuth oxyiodide with a similar structure as BOI-350, but having more iodine vacancies and a larger band gap, while the latter one can be given arise to an analogue of BOI-450(Bi_5O_7I) with less iodine vacancies and a smaller band gap. Therefore BOI-400 can be

regarded as a composites of two components, which is an intermediate of the transition from BOI-350 to BOI-450. Although the accurate composition of BOI-400 cannot be obtained, if we estimated the composition in according with a composite of BOI-350 and BOI-450, considering the Bi/I ratio of 4.38 in BOI-400, the composition of BOI-400 can be regarded as about 68.5% BOI-350 and 31.5% BOI-450.

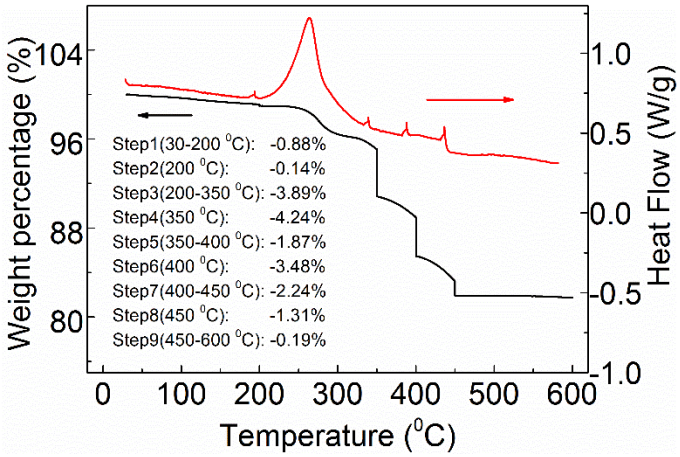

Fig. 3. Thermogravimetric (TG) and differential thermal (DT) curves of BOI-160.

To further understand the changes during calcinations of bismuth oxyiodide, a TG-DTA measurement under programming temperatures has been taken, as shown in Fig. 3. The weight loss below 200 °C can be attributed to the evaporation of bounded water. There is a significant loss of weight from 200-450 °C. Even holding at a certain temperature, iodine would continuously escape out and resulting in the decrease of weight, which is consistent with our above analyses. There are an obvious exothermic peak below 350 °C and an endothermic peak at about 450 °C, indicating the thermodynamic processes of the iodine escape and the phase transition are different. According to the theoretic estimation, the weight loss in the transformation from BiOI to Bi_5O_7I is 27.03%, and from $Bi_7O_9I_3$ to Bi_5O_7I is 9.57%. However, the weight loss from 200-450 °C in this work is about 17%, which could be overestimated than theoretic data because of the complicate nonstoichiometric relationship of these compounds.

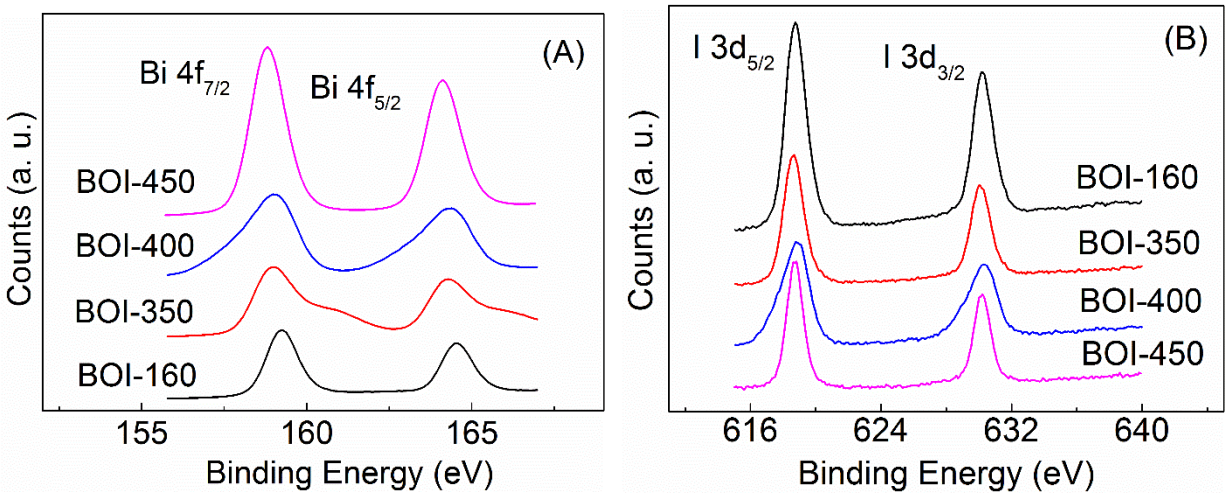

Fig. 4. XPS high-resolution Bi 4f (A) and I 3d (B) spectra of bismuth oxyiodide compounds.

XPS spectra were taken to investigate the chemical situations of elementary bismuth and iodine in the compounds. The binding energies at about 159 eV and 164 eV can be attributed to the Bi 4f7/2 and Bi 4f5/2, respectively.[28, 29] Increasing the calcination temperatures, these peaks downward shift slightly. It is understandable because with the loss of iodine, elementary bismuth is surrounded by more oxygen, which has a higher electronegativity than iodine. Moreover, there is little change of binding energies for I 3d5/2 and I 3d3/2 at 618.8 eV and 630.2 eV, respectively. This suggests that the chemical situation of iodine in the bismuth oxyiodide has not much altered even after the phase transition, which can be attributed to the presence of abundant oxygen and bismuth bounding with iodine. In addition, the unsymmetrical peaks for both Bi and I of BOI-400 indicates the presence of two kinds of species in this sample, which is in accordance to above results of XRD and DRS.

HRTEM images of BOI-400 were taken to further explore the interface of the two components in BOI-400, as shown in Fig. 5. It is notable that the microsphere structure has been destructed during calcinations. According to Fig. 5C, two kinds of fringe spacing are discernable in the particles of this bismuth oxyiodide, which are about 0.249 and 0.297 nm, respectively. The indistinct interface between the two components suggests an excellent contact in situ formed by calcination at a proper temperature.

According to the JCPDS card information, the (102) plane of tetragonal BiOI is about 0.301 nm, and the (004) plane of orthorhombic Bi_5O_7I is 0.287 nm. Because there lacks complete crystal information for $Bi_7O_9I_3$, and the presence of iodine vacancies would also induce alternations of the plane spacing, it is impossible to accurately attribute the two fringe spacing to their corresponding planes. Anyway, the presence of two components in the sample can be discerned in the TEM images.

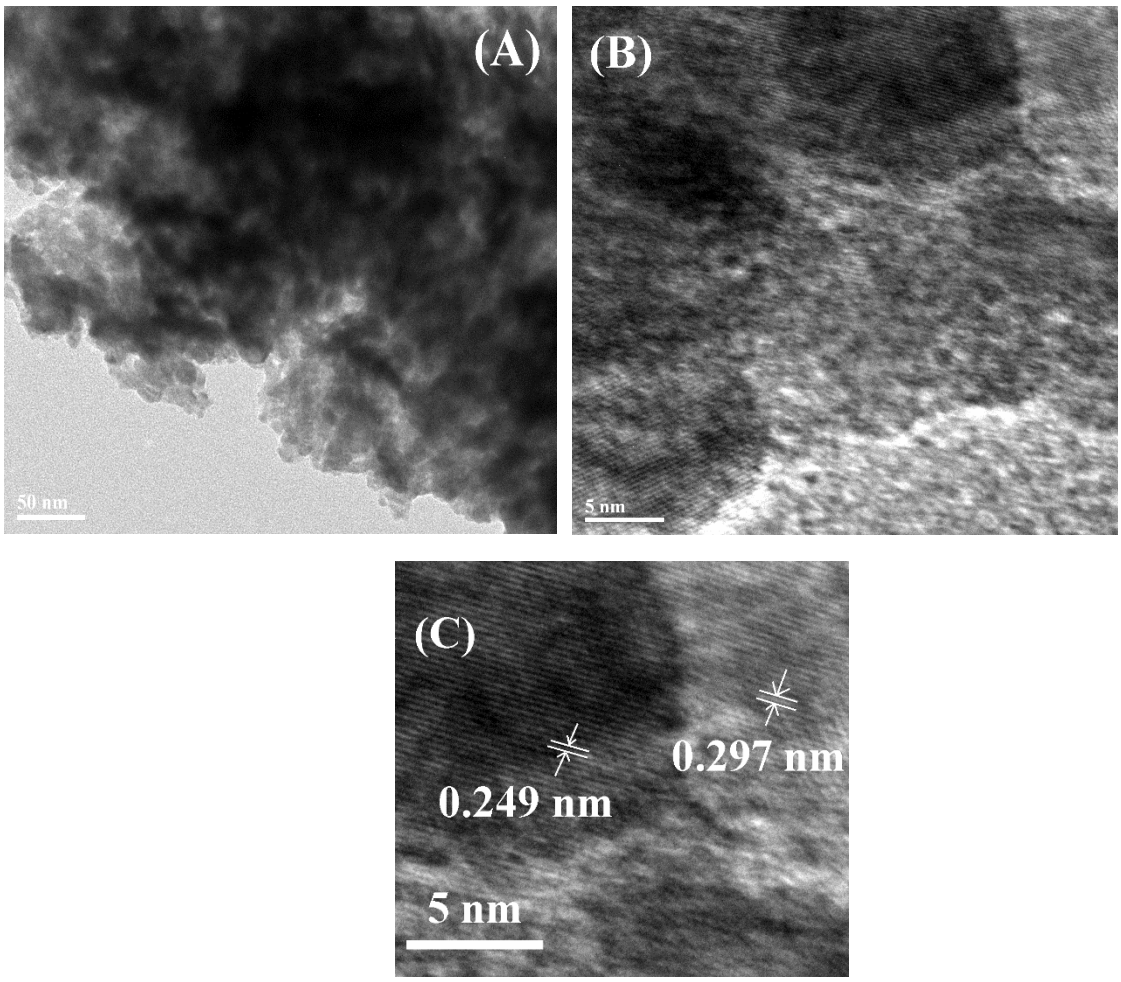

Fig. 5 (A) and (B) is HRTEM images of BOI-400, (C) is the magnified view of (B).

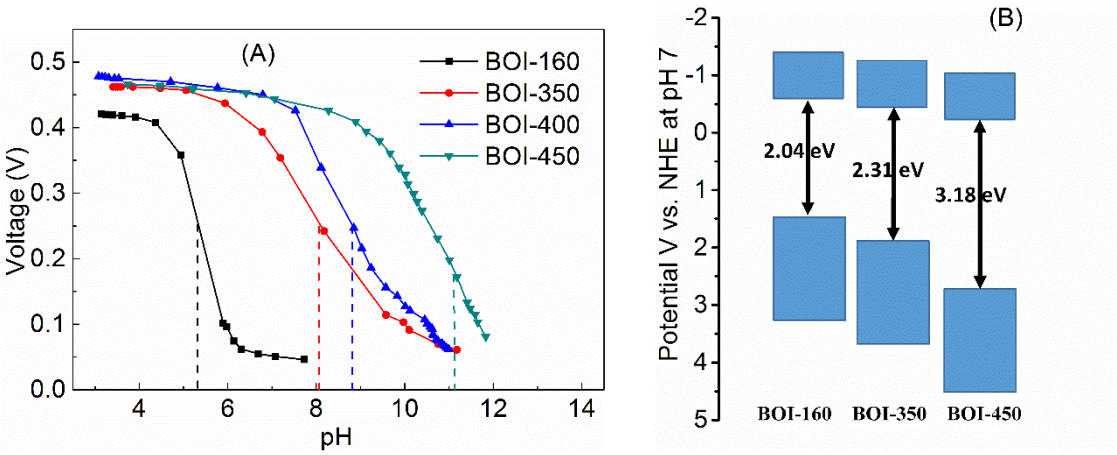

Fig. 6. (A) Photovoltage vs. suspension pH value measured for bismuth oxyiodides in 0.1 M KNO_3 in the presence of MV^{2+}; (B) Estimated band potentials for bismuth oxyiodides

The band potentials of these compounds can been estimated by the slurry method.[26] According to this method, the quasi-Fermi potential at any pH can be calculated according to Eq. 2, basing on the inflection points (pH_0) in the pH dependence of the photovoltage in the presence of a pH independent redox couple.

$$E_{FB}(pH) = E^0 - k(pH - pH_0) \qquad (2)$$

wherein E^0 is the standard reduction potential of the redox couple (eg. -0.54 V for MV^{2+}), k is generally 0.059 V/pH for semiconductors. The conduction band (CB) potential has been estimated according to the quasi-Fermi potential. When methylviologen (MV^{2+}) was used as the redox couple, the pH_0 obtained from Fig. 6 are located at 5.39, 8.05, 8.76 and 11.10 pH units for BOI-160, BOI-350, BOI-400 and BOI-450, respectively. Then, the CB potentials at pH 7 can be obtained as -0.63, -0.48, -0.44, -0.29 V vs. NHE for the four catalysts. It is notable that the positions of CBs shift anodic with the decrease of iodine contents. Considering their apparent band gap energies of 2.04, 2.31 and 3.18 eV obtained from DRS spectra, the valence band (VB) edge positions of BOI-160, BOI-350 and BOI-450 can be calculated as 1.41, 1.83 and 2.88 V vs. NHE, respectively. According to above DRS and CB potential measurements, the escape of iodine from bismuth oxyiodides would not only enlarge band

gaps, but also induce band positions downward shift and result in much more anodic valence bands.

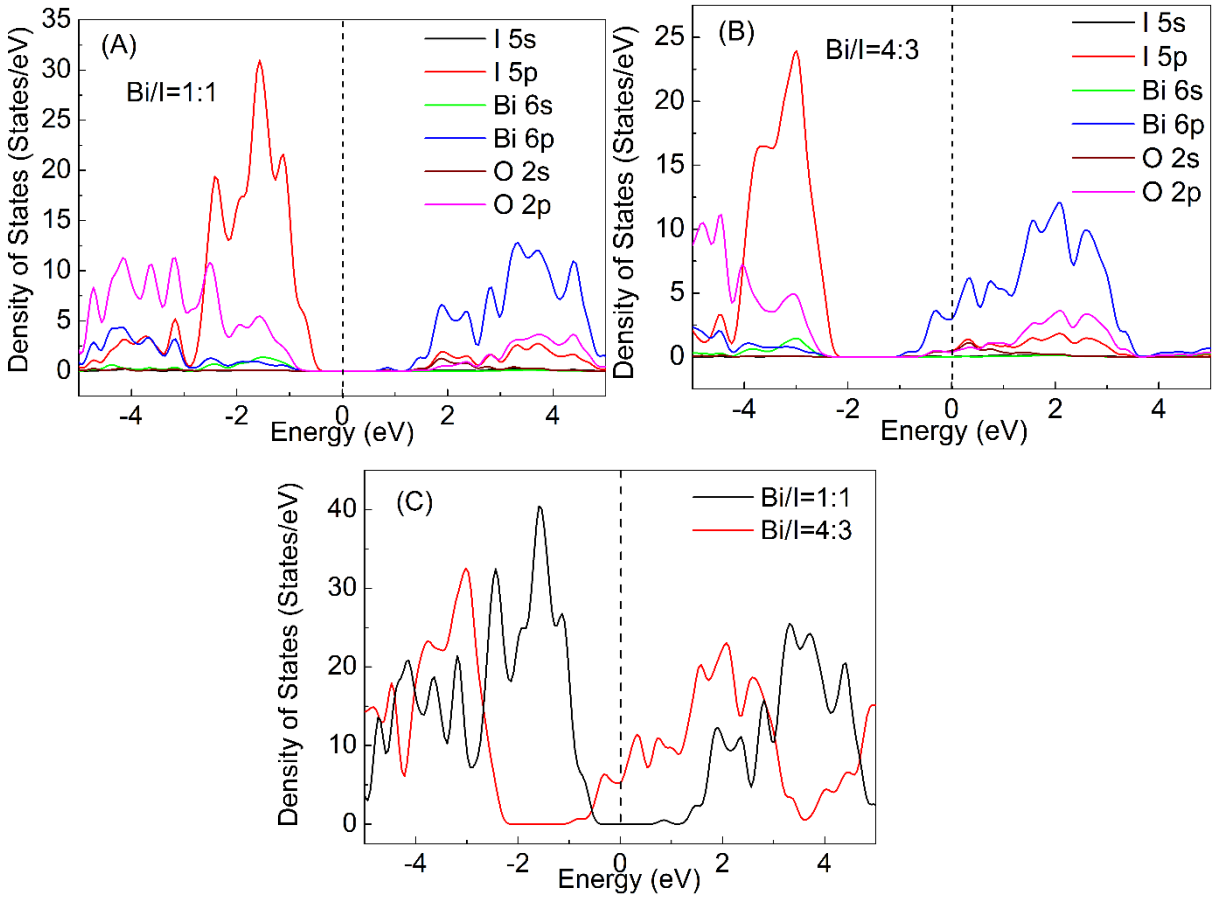

Fig. 7. Calculated partial density of states (PDOS) for bismuth oxyiodides with the ratio of Bi/I is (A) 1:1(BiOI) and (B) 4:3 (v-BiOI), and (C) their density of states.

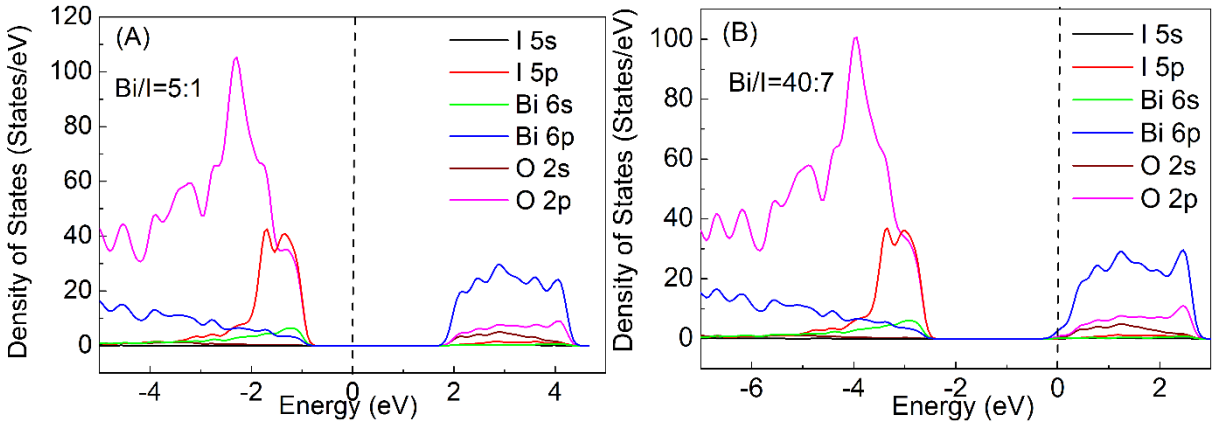

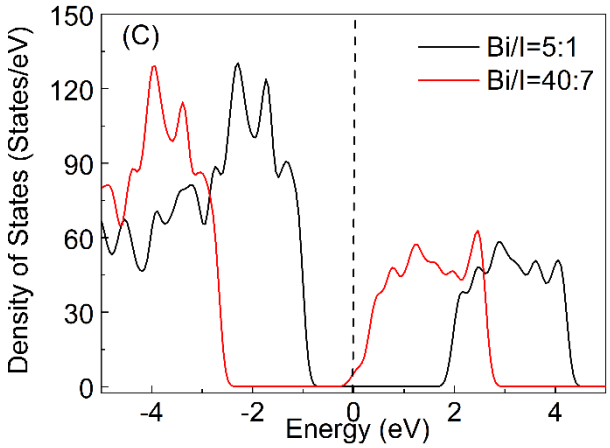

Fig. 8. Calculated partial density of states (PDOS) for bismuth oxyiodides with the ratio of Bi/I is (A) 5:1 (Bi_5O_7I) and (B) 40:7 (v-Bi_5O_7I), and (C) their density of states (DOS)

To understand the downward shift of band positions in bismuth oxyiodide compounds with iodine vacancies, we performed DFT calculations on BiOI, Bi_5O_7I and their corresponding compounds with iodine vacancies (Bi/I=4/3, denoted as v-BiOI; Bi/I=40:7, denoted as v-Bi_5O_7I) by Quantum ESPRESSO package. The calculated band gaps for v-BiOI and v-Bi_5O_7I is about 1.62 eV and 2.32 eV, slightly larger than 1.35 eV for BiOI and 2.30 eV for Bi_5O_7I. The underestimated band gap is the inherent shortcoming of DFT methods. The results of band gaps suggest that the band gap would increase with the escape of iodine in the lattice. The calculated partial density of states (PDOS) and density of states (DOS) were shown in Fig. 7 and Fig. 8. The compositions of CB and VB are similar for the compounds with or without iodine vacancies. According to Fig. 7, the top of valence band (TVB) of BiOI and v-BiOI mainly consists of I_{5p} and O_{2p} orbitals, with slight contributions from Bi_{6s}. The bottom of CB (BCB) is dominated by Bi_{6p} orbital, accompanying with the small contributions from O_{6p} and I_{5p} orbitals. However, compositions of CB and VB of Bi_5O_7I is quite different with BiOI. From Fig. 8, the TVB of Bi_5O_7I and v-Bi_5O_7I is dominated by O_{2p} and I_{5p} orbitals, while their BCB is mainly comprised of Bi_{6p}, with a few contributions from O_{2p} and O_{2s} orbitals. It is obvious that without iodine vacancies, both bismuth oxyiodides display a p-type semiconductor behavior, because the Fermi

level is closer to their TVB. However, the band positions shift downwards when iodine vacancies presenting in the lattice, and it would lead to higher oxidation powerful photogenerated holes on VB. This is consistent with our experimental results from the slurry method. Moreover, with the downward shift of band positions, the Fermi levels of bismuth oxyiodides with iodine vacancies become closer to BCB, indicating the semiconductor behavior has changed from p type to n type. Such transition would make electrons dominate in the semiconductor and enhance the mobility of electrons. Therefore the presence of iodine vacancies in the lattice of bismuth oxyiodides could alter their electronic structures, which basically influence their photocatalytic performance.

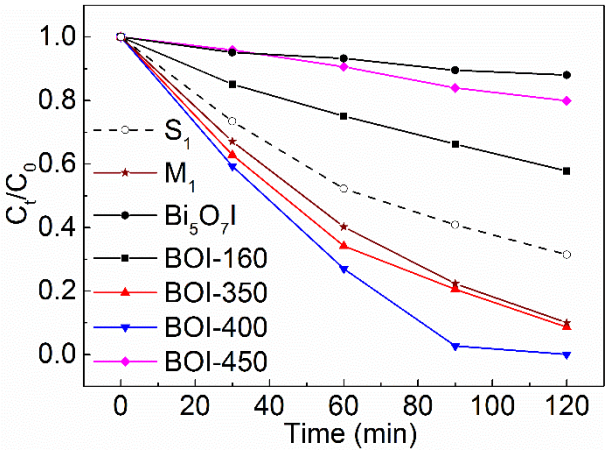

Fig. 9 Visible light photocatalytic degradation of phenol over various bismuth oxyiodides, in which M_1 is a mixture of 68.5% BOI-350 and 31.5% BOI-450, S_1 is the calculated sum value of BOI-350 and BOI-450 with the same ratio as M_1. (catalyst dosage: 1g/L, λ>400 nm)

The visible light photocatalytic activities of bismuth oxyiodide catalysts for phenol degradation were investigated and the results are shown in Fig. 9. As-prepared BOI-160 shows moderate catalytic activity, only 42% phenol reduction achieved after 120 min irradiation. Bi_5O_7I and BOI-450 have poor visible light activity, with the phenol reduction as low as 11% and 20% in 120 min, respectively. It can be attributed to their low absorption in the range of visible light due to their large band gap energies. Yet the calcined bismuth oxyiodides below 450 °C display significantly enhanced catalytic activity.

The reduction of phenol is 91.4% in 120 min over BOI-350. Such high activity can be ascribed to the presence of iodine vacancies, which resulting in a larger band gap, more anodic valence band and the transition of semiconductor behaviors. Therefore, the photogenerated holes on BOI-350 possess a higher oxidation power, while the photogenerated electrons have a faster mobility, both of which would contribute to a better photocatalytic performance.[30, 31]

BOI-400 displays the best photocatalytic activity, more than 97.4% phenol reduction achieved after only 90 min irradiation. The excellent photocatalytic activity must be caused by its special heterojunction structure. To support the charge transfer between various components in BOI-400, the photocatalytic activity of a mixture with 68.5% BOI-350 and 31.5% BOI-450 was measured (Curve M_1). The phenol degradation efficiency is almost the same as that with 100% BOI-350, while much higher than the calculated sum of BOI-350 and BOI-450 with the same ratios (curve S_1). The result suggests that there is an interparticle electron transfer (IPET) effect between the coupled semiconductors of BOI-350 and BOI-450, because they have suitable CB and VB positions for the migration of photogenerated electrons and holes, as shown in Fig. 6B. Therefore, with the enhanced charge separation and suppressed recombination, the mixture catalysts demonstrated an enhanced photocatalytic activity.[1, 32, 33] Although we cannot determine the accurate compositions of the two components in BOI-400, they must possess matched band positions as BOI-350 and BOI-450 according to the consecutive changes of Bi/I ratio and band potential shifts. Several radical scavenges were employed in phenol degradation to further understand the charge transfer process in excited BOI-400, and the results are shown in Fig. 10. The typical hydroxyl radical scavengers of methanol and 2-propanol have little influence on the photocatalytic activity, even at a concentration as high as 0.1M. It indicates that •OH in the bulk solution does not play the crucial role for the photocatalytic

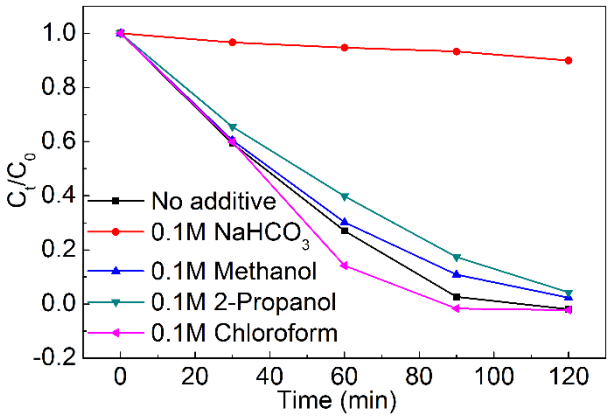

Fig. 10. The decrease of phenol as a function of irradiation time in BOI-400 suspension under visible irradiation (λ >400 nm) with or without scavengers.

degradation of phenol. This could be attributed to that holes accumulating on the VB of the semiconductor possess potentials not anodic enough to oxidize OH^- into •OH (•OH/OH^-=+1.99 V). It is interesting that the addition of 0.1 M chloroform can promoted the reaction. This can be rationalized that the reaction rate constant of chloroform with electrons is as high as 3×10^{10} $M^{-1}S^{-1}$, even faster than that of oxygen (1.9×10^{10} $M^{-1}S^{-1}$).[34] Therefore the contribution of O_2^-• radicals to phenol degradation is not significant. Basic carbonate anions are typical scavenger for the adsorbed •OH radicals or holes.[35, 36] It was found that the addition of $NaHCO_3$ significantly suppressed the photocatalytic degradation of phenol, suggesting the main active species for phenol degradation in the irradiated BOI-400 suspension was photogenerated holes. Hence, most possible relative positions of band potentials of the two components in BOI-400 can be plotted in Scheme 1. In the excited BOI-400, the photogenerated electrons would concentrate at the conduction band of the wider band gap semiconductor with a potential more negative than -0.29 V, being readily scavenged by O_2(O_2/O_2^-=-0.28 V). Simultaneously, holes with a potential more anodic than +1.83 V would accumulated at the valence band of the component with narrower band gap. Moreover, the well alloyed interface formed during calcination makes charge transfer between two components more facile. Because of the well alloyed interface and

the efficient photogenerated charge separation, BOI-400 displays an excellent photocatalytic performance, and is promising for the practical applications in pollutants removal.

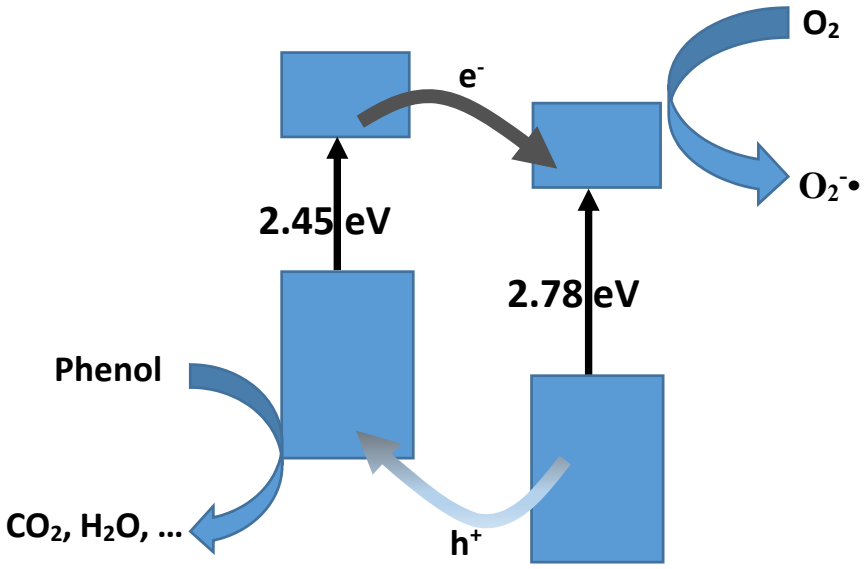

Scheme 1 Schematic diagram for the charge separation in the irradiated BOI-400.

Conclusions

Upon calcination of bismuth oxyiodide ($Bi_7O_9I_3$) synthesized from solvothermal method, iodine atoms continuously escape out, resulting in the generation of iodine vacancies, bringing the phase transition above 350 °C and in situ forming a heterojunction with excellent visible light photocatalytic activity at 400 °C. According to DRS analyses, band potential measurements or theoretic calculations, it is revealed that the presence of iodine vacancies would increase band gaps, make downward shifts of band potentials and induce the change of semiconductor behavior from p type to n type. BOI-400 is composed by two components with well-matched band potentials and well contact interfaces, resulting in an efficient charge separation and excellent photocatalytic performance. We can anticipated to develop novel bismuth oxyiodide photocatalysts with desirable performance by regulating the electronic structures and fabricating heterojunctions through simultaneously controlling the extent of phase transition and the amount of iodine vacancies.

Acknowledgments

This work is financially supported by National Natural Science Foundation of China (No. 21377084) and Shanghai Municipal Natural Science Foundation (No. 13ZR1421000). We gratefully acknowledge the support and valuable suggestions in XRF and XPS measurements by Ms. Lingling Li and Ms. Qianqian Hu of the Instrumental Analysis Center of Shanghai Jiao Tong University.

† Electronic supplementary information (ESI) available: EPR spectra and measurement method, Time dependent TGA curve. See DOI:

References

1. M. Long, W. Cai, J. Cai, B. Zhou, X. Chai and Y. Wu, *J Phys Chem B* 2006, **110**, 20211-20216.
2. N. Zhang, R. Ciriminna, M. Pagliaro and Y. J. Xu, *Chem Soc Rev*, 2014, **43**, 5276-5287.
3. J. Henle, P. Simon, A. Frenzel, S. Scholz and S. Kaskel, *Chem Mater*, 2007, **19**, 366-373.
4. X. Xiao, C. Liu, R. Hu, X. Zuo, J. Nan, L. Li and L. Wang, *J Mater Chem*, 2012, **22**, 22840.
5. Q. C. Liu, D. K. Ma, Y. Y. Hu, Y. W. Zeng and S. M. Huang, *ACS Appl Mater Interfaces*, 2013, **5**, 11927-11934.
6. X. Zhang, Z. H. Ai, F. L. Jia and L. Z. Zhang, *J Phys Chem C*, 2008, **112**, 747-753.
7. L. Ye, L. Tian, T. Peng and L. Zan, *J Mater Chem*, 2011, **21**, 12479–12484.
8. X. Chang, J. Huang, Q. Tan, M. Wang, G. Ji, S. Deng and G. Yu, *Catal Commun*, 2009, **10**, 1957-1961.
9. X. Xiao and W. D. Zhang, *J Mater Chem*, 2010, **20**, 5866-5870.
10. X. Xiao and W. D. Zhang, *RSC Adv*, 2011, **1**, 1099–1105.
11. S. Sun, W. Wang, L. Zhang, L. Zhou, W. Yin and M. Shang, *Environ Sci Technol*, 2009, **43**, 2005-2010.
12. J. Cao, X. Li, H. Lin, B. Xu, B. Luo and S. Chen, *Mater Lett*, 2012, **76**, 181-183.
13. E. Keller, V. K. m. I, M. Schmidt and H. Oppermann, *Z Kristallogr*, 2002, **217**, 256–264.
14. L. Guangshe, L. Liping and Z. Jing, *Sci China Chem*, 2011, **54**, 876–886.
15. M. V. Ganduglia-Pirovano, A. Hofmann and J. Sauer, *Surf Sci Rep*, 2007, **62**, 219-270.
16. F. Banhart, J. Kotakoski and A. V. Krasheninnikov, *ACS Nano*, 2010, **5**, 26-41.

17. X. Pan, M. Q. Yang, X. Fu, N. Zhang and Y. J. Xu, *Nanoscale*, 2013, **5**, 3601-3614.
18. X. Zhang and L. Zhang, *J Phys Chem C*, 2010, **114**, 18198-18206.
19. C. L. Yu, F. F. Cao, X. Li, and K. Yan, *Nonferr Metal Sci Eng*, 2011, **2**, 86-91.
20. A. Kubacka, M. Fernandez-Garcia and G. Colon, *Chem Rev*, 2012, **112**, 1555-1614.
21. M. Long, W. Cai and H. Kisch, *J Phys Chem C*, 2008, **112**, 548-554.
22. X. F. Wang, S. F. Li, Y. Q. Ma, H. G. Yu and J. G. Yu, *J Phys Chem C*, 2011, **115**, 14648-14655.
23. H. G. Yu, R. Liu, X. Wang, P. Wang and J. G. Yu, *Appl Catal B*, 2012, **111-112**, 326-333.
24. D. F. Wang, Z. G. Zou and J. H. Ye, *Chem Mater*, 2005, **17**, 3255-3261.
25. H. G. Kim, E. D. Jeong, P. H. Borse, S. Jeon, K. Yong, J. S. Lee, W. Li and S. H. Oh, *Appl Phys Lett*, 2006, **89**, 064103
26. A. M. Roy, G. C. De, N. Sasmal and S. S. Bhattacharyya, *Int J Hydrogen Energy*, 1995, **20**, 627-630.
27. P. Giannozzi, S. Baroni, N. Bonini, M. Calandra, R. Car, C. Cavazzoni, D. Ceresoli, G. L. Chiarotti, M. Cococcioni, I. Dabo, A. Dal Corso, S. de Gironcoli, S. Fabris, G. Fratesi, R. Gebauer, U. Gerstmann, C. Gougoussis, A. Kokalj, M. Lazzeri, L. Martin-Samos, N. Marzari, F. Mauri, R. Mazzarello, S. Paolini, A. Pasquarello, L. Paulatto, C. Sbraccia, S. Scandolo, G. Sclauzero, A. P. Seitsonen, A. Smogunov, P. Umari and R. M. Wentzcovitch, *J Phys: Condens Matter*, 2009, **21**, 395502.
28. Z. Zhao, F. Liu, L. Zhao and S. Yan, *Appl Phys A*, 2010, **103**, 1059-1065.
29. J. Cao, B. Xu, H. Lin, B. Luo and S. Chen, *Dalton Trans*, 2012, **41**, 11482-11490.
30. M. Long, W. Cai, Z. Wang and G. Liu, *Chem Phys Lett*, 2006, **420**, 71-76.
31. M. Mrowetz, W. Balcerski, A. J. Colussi and M. R. Hoffmann, *J Phys Chem B*, 2004, **108**, 117269-117273.
32. D. Robert, *Catal Today*, 2007, **122**, 20-26.
33. N. Serpone, P. Maruthamuthu, P. Pichat, E. Pelizzetti and H. Hidaka, *J Photochem Photobio A: Chem*, 1995, **85**, 247-255.
34. G. V. Buxton, C. L. Greenstock, W. P. Helman and A. B. Ross, *J Phys Chem Ref Data*, 1988, **17**, 513-886.
35. Y. Wang, Y. Wang and Y. Gao, *React Kinet Mech Catal*, 2010, **99**, 485–491.
36. K. Sayama and H. Arakawa, *J Chem Soc, Faraday Trans*, 1997, **93**, 1647-1654.

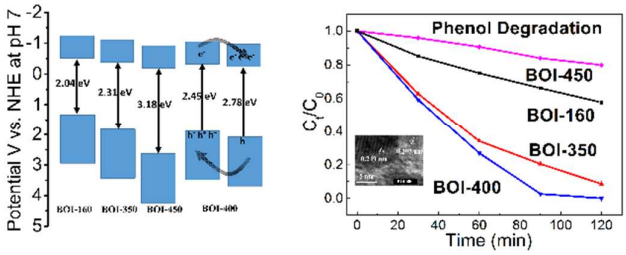

Iodine vacancies in bismuth oxyiodides generated by calcination contribute to the increased band gaps and more anodic valance band potentials. Well contact interface between two components, accompanying with iodine vacancies result in the efficient photocatalytic performance of bismuth oxyiodides when calcined at 400 ^{0}C.